Quantum theory of the coherently pumped micromaser: Model and steady-state solution

István Németh* and János A. Bergou†
Department of Physics, Hunter College, 695 Park Avenue, New York, New York 10021, USA
(Received 10 November 2003; revised manuscript received 1 June 2005; published 26 August 2005)

A detailed theoretical and experimental study of the atom-field interaction starting from first principles was made possible by the realization of the single-atom micromaser. The situation is very close to the ideal case of a single two-level atom interacting with a single quantized mode of a superconducting cavity. In spite of the considerable amount of work devoted to the study of the micromaser, it still remains to be established how the system behaves under coherent pumping. We present a comprehensive study of the coherently pumped micromaser; we develop an *analytic* method to obtain the steady-state solution of the master equation governing the time evolution of the cavity field. We illustrate this method with a simple example and present results for the photon distribution and purity of the steady state of the coherently pumped micromaser.

DOI: 10.1103/PhysRevA.72.023823 PACS number(s): 42.50.Pq, 42.65.Sf, 03.65.Yz, 42.50.Dv

I. INTRODUCTION

There are only a handful of systems in physics that can be studied starting from first principles using exact theoretical methods and, at the same time, can be investigated under experimental conditions approaching the idealized theoretical one. The single-atom maser or micromaser provides such an example, making a detailed study of the atom-field interaction possible. The situation realized in a micromaser is very close to the ideal case of a single two-level atom interacting with a single quantized mode of a cavity field.

In the early works devoted to the theory of the microscopic maser (Filipowicz *et al.* [1,2]) the case of incoherent pumping was investigated where two-level atoms, excited to their upper level, randomly interact with a single quantized mode of a superconducting cavity (for a recent review see [3]). It was found that the field mode evolves toward a steady state when the average lifetime of a photon in the field mode is larger than the mean time between the interactions. As the pump rate increases the steady state goes through thresholds that resemble first-order phase transitions. This remarkably simple system, which exhibits a rich structure of phase transitions, soon found various experimental realizations [4–8]. State-of-the-art experimental techniques made it possible to build superconducting high-Q niobium microcavities which could maintain large photon numbers. In recent experiments, values of the quality factor as high as 3×10^{10} have been achieved for the resonant mode, corresponding to an average lifetime of a photon in the cavity of 0.2 s. In the experiments rubidium Rydberg atoms, selectively pumped by laser excitation into the upper level of the maser transition, were used. A consequence of the high-Q value is that the photon lifetime is much longer than the interaction time of an atom with the maser field. Therefore, during the time the atom passes through the cavity the only change in the cavity field is due to the atom-field interaction which can be adequately treated then using the Jaynes-Cummings model [9,10]. Remarkable quantum effects have been predicted and observed such as the collapse and revival of Rabi oscillations [6], maser action without inversion [11], and the quantum clock [12]. Also, various uniquely quantum-mechanical states of the field, including entangled states [13], trapping states [2,14,15], tangent and cotangent states [16,17], sub-Poissonian photon statistics [7], and even the Fock state [18,19], have been generated. These findings established the significance of the micromaser as a testing ground for fundamental principles.

Although considerable work, both theoretical and experimental, has been carried out on this system, with a few exceptions noted below, most cases involved incoherent pumping. As a result, the density matrix describing the field remained diagonal for all times if the initial state of the field was diagonal (an initial condition experimentally realizable, allowing the system to relax until no transient nondiagonal entries are left). Therefore, investigations of phase diffusion [20,21] and the spectrum [22–28] of the micromaser involved both the creation of nondiagonal density matrix entries and the study of their decay. The creation of nondiagonal entries of the density matrix can be achieved in two ways: either by injecting a preselected phase into the micromaser or by post-selecting a phase via the detection of the exiting atoms [29–34]. In our work we use the preselection of phase, which is achieved by injecting atoms, initially prepared in a proper form of the atomic coherence, into the micromaser cavity (coherent pumping). This line of investigations was started by the work of Krause *et al.* [29], describing how the phase of the atomic coherence is transferred to the field in the limit of weak atom-field coupling. Slosser *et al.* [16,17] found that the field of a coherently pumped lossless micromaser evolves toward pure states, called tangent and cotangent states. Casagrande *et al.* [35–37] studied the dynamics of a coherently driven micromaser (a micromaser continuously driven by a resonant coherent field and pumped by atoms injected in superposition states) using quantum jump techniques, and recently Lougovski *et al.* [38] investigated the dynamics of a strongly driven micromaser (a micromaser where the pumping atoms are strongly driven by a resonant classical field during their traverse through the cavity) and presented a time-dependent analytic solution. Despite all of this progress, a comprehensive study of the

*Electronic address: istvan.nemeth@hunter.cuny.edu
†Electronic address: janos.bergou@hunter.cuny.edu

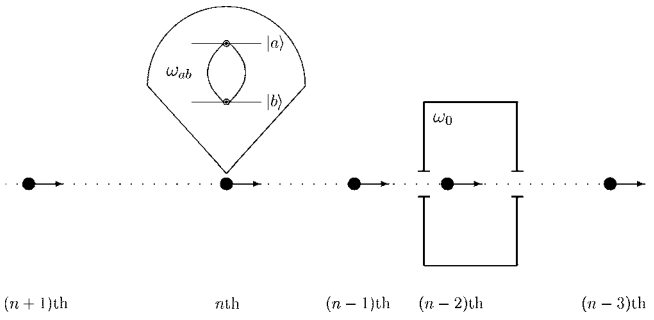

FIG. 1. Micromaser pumped by two-level atoms initially prepared in a coherent superposition of their upper level $|a\rangle$ and lower level $|b\rangle$.

"conventional" coherently pumped micromaser is yet to be given. Especially interesting problems are the relation of the phase of the steady-state field to that of the driving atoms under general conditions, including the case of off-resonant pumping, and developing analytic methods for this highly nonlinear system. In a series of articles our goal is to provide a comprehensive study of the coherently pumped micromaser focusing on these questions.

In this article, the first in the series, we introduce the model of the coherently pumped micromaser and provide the analytic steady-state solution. The work is organized as follows. Starting in Sec. II we present the master equation governing the time evolution of the electromagnetic field inside the micromaser cavity and discuss, in detail, the control parameters of the model. Then in Sec. III we discuss the large-scale structure of the field density matrix and present an *analytic* method to obtain the steady-state solution of the master equation. (We illustrate the method with an example in the Appendix.) In Sec. IV we present results for the photon distribution and for the purity of the steady state of the coherently pumped micromaser. We conclude with a brief summary.

II. MODEL AND THE FIELD MASTER EQUATION

A coherently pumped micromaser, illustrated in Fig. 1, consists of a stream of two-level atoms (upper level a and lower level b) and a single mode of a high-Q micromaser cavity. The atoms, initially prepared in a proper form of the atomic coherence, are randomly injected into the micromaser cavity at a rate r low enough that at most one atom at a time is present inside the cavity. The mean time between consecutive atoms is T where $T=1/r$. In the cavity the atoms interact with a single mode of the micromaser field for a time period of $\tau \ll T$ where τ is the transit time of a single atom through the micromaser cavity. We assume that the nth atom is injected at time t_n, with the initial density matrix

$$\rho_{atom}^{(n)}(t_n) = \begin{pmatrix} \rho_{aa} & \lambda\rho_{ab}e^{-i\nu t_n} \\ \lambda\rho_{ba}e^{i\nu t_n} & \rho_{bb} \end{pmatrix}. \tag{2.1}$$

Here ρ_{aa} and $\rho_{bb}=1-\rho_{aa}$ are the populations and $\rho_{ab}=\rho_{ba}^{*}=|\rho_{ab}|e^{i\varphi_{ab}}$ with $\rho_{ab}=\sqrt{\rho_{aa}\rho_{bb}}$ are the maximally allowed coherences for a given population. (For a discussion of the preparation of atoms in such a state see [39].) Furthermore, ν is the frequency of the classical field used to prepare the atomic coherence, hereafter referred to as the injected signal frequency. This frequency is not necessarily the same as the atomic transition frequency ω_{ab} [$=(E_a-E_b)/\hbar$, where E_a and E_b are the energies of states $|a\rangle$ and $|b\rangle$, respectively]. The parameter λ ($0\leqslant\lambda\leqslant 1$) determines the degree of the injected coherence. If $\lambda=0$, no atomic coherence, and if $\lambda=1$, the maximal atomic coherence is injected into the micromaser. Introducing λ allows us to continuously scale our model from incoherent to fully coherent pumping.

Various methods that take proper account of the arrival times statistic of the pumping atoms were developed to obtain the master equation for the density operator of the cavity field [40–43]. For nonresonant pumping and Poissonian arrivals they all lead to the same master equation, which is given explicitly by Orszag [44]. In the interaction picture—after transforming the explicitly time-dependent terms away using

$$\rho_S(t) = e^{-i\mathbf{a}^{\dagger}\mathbf{a}(\nu t+\varphi_g-\varphi_{ab}+\pi/2)}\rho(t)e^{i\mathbf{a}^{\dagger}\mathbf{a}(\nu t+\varphi_g-\varphi_{ab}+\pi/2)}, \tag{2.2}$$

where $\rho_S(t)$ [$\rho(t)$] is the density operator of the field in the Schrödinger [interaction] picture—the master equation reads as

$$\begin{aligned}\frac{d\rho_{k,l}(t')}{dt'} &= [A_{k,l,-1,-1}\rho_{k-1,l-1}(t') + A_{k,l,-1,0}\rho_{k-1,l}(t') \\ &\quad + A_{k,l,0,-1}\rho_{k,l-1}(t') - A_{k,l,0,0}^{(1)}\rho_{k,l}(t')] \\ &\quad - [A_{k,l,0,0}^{(2)}\rho_{k,l}(t') + A_{k,l,0,1}\rho_{k,l+1}(t') \\ &\quad + A_{k,l,1,0}\rho_{k+1,l}(t') - A_{k,l,1,1}\rho_{k+1,l+1}(t')].\end{aligned} \tag{2.3}$$

Here $\rho_{k,l}=\langle k|\rho|l\rangle$ are the matrix elements of the density operator of the cavity field in the number state basis, with k, l non-negative integers, and we introduced the notation

$$A_{k,l,-1,-1} = \left(\frac{N_{ex}}{2}(1+u)S_kS_l + \bar{n}_{th}\sqrt{kl}\right), \tag{2.4a}$$

$$A_{k,l,-1,0} = \left(\frac{N_{ex}}{2}\lambda\sqrt{1-u^2}S_kC_l\right), \tag{2.4b}$$

$$A_{k,l,0,-1} = \left(\frac{N_{ex}}{2}\lambda\sqrt{1-u^2}C_k^{*}S_l\right), \tag{2.4c}$$

$$A_{k,l,0,0}^{(1)} = \left(\frac{N_{ex}}{2}(1-u)(1-C_k^{*}C_l) + i\Delta(k-l) + (\bar{n}_{th}+1)\frac{k+l}{2}\right), \tag{2.4d}$$

$$A_{k,l,0,0}^{(2)} = \left(\frac{N_{ex}}{2}(1+u)(1-C_{k+1}C_{l+1}^{*}) + \bar{n}_{th}\frac{(k+1)+(l+1)}{2}\right), \tag{2.4e}$$

$$A_{k,l,0,1} = \left(\frac{N_{ex}}{2}\lambda\sqrt{1-u^2}C_{k+1}S_{l+1}\right), \tag{2.4f}$$

$$A_{k,l,1,0} = \left(\frac{N_{ex}}{2} \lambda \sqrt{1-u^2} S_{k+1} C_{l+1}^* \right), \tag{2.4g}$$

$$A_{k,l,1,1} = \left(\frac{N_{ex}}{2} (1-u) S_{k+1} S_{l+1} + (\bar{n}_{th}+1) \sqrt{(k+1)(l+1)} \right), \tag{2.4h}$$

where

$$C_k = \cos(\sqrt{n_0^2+k}\Theta) + i \frac{n_0}{\sqrt{n_0^2+k}} \sin(\sqrt{n_0^2+k}\Theta), \tag{2.5a}$$

$$S_k = \frac{\sqrt{k}}{\sqrt{n_0^2+k}} \sin(\sqrt{n_0^2+k}\Theta), \tag{2.5b}$$

satisfying $C_k^* C_k + S_k^2 = 1$. The frequency we used to go into the interaction picture, Eq. (2.2), is the injected signal frequency ν and not the frequency of the empty cavity-field eigenmode ω_0. This choice was suggested by the theory of the classical forced oscillations, where a system is driven by an external force and the frequency of the resultant steady oscillation equals that of the driving. (Similar frequency locking was observed by Carty and Sargent [45,46] using the semiclassical method to investigate the interaction of a single-mode electric field with homogeneously broadened two-level medium prepared in a coherent superposition of energy eigenstates.)

In Eqs. (2.3)–(2.5) we used the following parameters. The time is scaled to the cavity decay time,

$$t' = \Gamma t, \tag{2.6}$$

where Γ is the cavity-damping constant. It arises due to the coupling of the cavity field to the environment, which is modeled by a reservoir in thermal equilibrium where the mean number of thermal photons is $\bar{n}_{th}$, and

$$N_{ex} = \frac{r}{\Gamma} = \frac{1}{\Gamma T} \tag{2.7}$$

gives the number of atoms passing through the cavity during the cavity decay time $1/\Gamma$. Furthermore,

$$u = \rho_{aa} - \rho_{bb} \tag{2.8}$$

is the atomic inversion parameter,

$$\Delta = \frac{\omega_0 - \nu}{\Gamma} \tag{2.9}$$

is the scaled detuning which gives the phase shift accumulated during the cavity decay time between the oscillation of the empty cavity field and the injected signal,

$$\Theta = |g|\tau \tag{2.10}$$

determines the interaction phase of a single atom and the cavity field,

$$n_0 = \frac{\omega_0 - \omega_{ab}}{2|g|} \tag{2.11}$$

describes the effective photon number shift due to the detuning of the empty cavity frequency and the atomic transition frequency, and $|g|$ is the magnitude of the complex atom-field coupling constant, $g = |g| e^{i\varphi_g}$, appearing in the Jaynes-Cummings Hamiltonian.

We want to emphasize that our model contains two parameters related to detuning. The first one n_0 is the consequence of the frequency mismatch between ω_0 and ω_{ab}, the frequencies of the empty cavity field and the atomic transition, respectively. The result of n_0 is an effective photon number shift as it can be seen from Eq. (2.5). The other detuning related parameter Δ is due to the difference between ω_0 and the frequency of the injected signal ν. Δ and n_0 are independent parameters; their value can be chosen separately to control different aspects of the model. However, the preparation of the atomic coherence is most effective when $\omega_{ab} = \nu$. In this case $n_0 = (\Gamma/2|g|)\Delta$, so there is just one independent detuning parameter left in the model. Nevertheless, for the sake of full generality we treat n_0 and Δ as independent parameters.

Before we proceed any further, we list all the parameters used to set up the model: u, φ_{ab}, ω_{ab}, ν, λ, $|g|$, φ_g, ω_0, τ, r, Γ, and $\bar{n}_{th}$. However, as we can see from Eq. (2.3), $\rho(t')$ does not depend directly on all of these 12 parameters; some only appear in combinations with others. Therefore, it is important to identify the minimal set of parameters which uniquely determine $\rho(t')$. These control parameters, as read out from Eqs. (2.3) and (2.4), are N_{ex}, u, λ, Θ, n_0, Δ, and $\bar{n}_{th}$. Neither φ_{ab} nor φ_g appears in Eq. (2.3); they only introduce a constant phase shift between the initial values of ρ_S and ρ, Eq. (2.2), and therefore they can be eliminated from our further investigation (they can simply be set to zero). In conclusion, we can say that the solution to Eq. (2.3), besides time, depends on

$$\boldsymbol{\beta} = (N_{ex}, u, \lambda, \Theta, n_0, \Delta, \bar{n}_{th}), \tag{2.12}$$

where $\boldsymbol{\beta}$ is a vector in the seven-dimensional parameter space of the model. We can summarize this by writing $\rho(t') = \rho(\boldsymbol{\beta}, t')$. It is important to notice that in $\boldsymbol{\beta}$ all the parameters are dimensionless quantities and that we have two parameters λ and Δ, which are exclusive to the coherent pumping. Furthermore, in the case when the thermal reservoir is at zero temperature the mean number of thermal photons in the cavity is zero, $\bar{n}_{th} = 0$, and the number of the independent parameters reduces to 6.

Before we present the steady-state solution we would like to point out why is it so hard to solve the master equation (2.3). In the case of incoherent pumping ($\lambda = 0$), $\rho_{k,l}(\boldsymbol{\beta}, t')$ is only coupled to the entries in the same diagonal. In the case of coherent pumping ($\lambda \neq 0$), however, $\rho_{k,l}(\boldsymbol{\beta}, t')$ is also coupled to the entries in the neighboring diagonals, making it impossible to use the solution techniques of the incoherently pumped micromaser. For this case, then, we must develop a method which handles the whole field density matrix simultaneously. Therefore, we start the next section with a brief

discussion of the large-scale structure of the density matrix for coherent pumping and then introduce the analytic solution technique.

III. STEADY-STATE, ANALYTIC SOLUTION

A. Field density matrix of the coherently and nonresonantly pumped lossy micromaser

The steady state formed in a micromaser is the result of two competing processes: the pumping and the decay due to the cavity losses. Under general conditions in the absence of either process a steady state cannot be reached (except, of course, the vacuum state). However, if in the absence of a thermal reservoir (decay process) we restrict the interaction phase Θ in such a way that the coupling between given rows and columns of the field density matrix cancels, a steady state will be reached. The restriction imposed on Θ leads to the appearance of the trapping states which were first introduced for the incoherently pumped micromaser by Filipowicz *et al.* [1] and Meystre *et al.* [14]. From Eq. (2.3) we see that trapping states can be generated in the coherently and nonresonantly pumped micromaser, as well by satisfying

$$S_{n_q+1} = 0, \quad q = 1,2,3, \ldots , \tag{3.1}$$

where n_q is the non-negative integer representing the indices for which the coupling between given rows and columns of the field density matrix is terminated. In this case the field density matrix is partitioned into noninteracting blocks, illustrated in Fig. 2, which evolve independently. The downward and upward trapping states known from the theory of the incoherently pumped micromaser [14] are located at the upper left and lower right corners of the partitions along the main diagonal of the field density matrix. Equivalently, we can also say that the trapping states create the partitions of the field density matrix. Using the definition of S_k, Eq. (2.5b), the condition imposed on the interaction phase by Eq. (3.1) is

$$\Theta = \frac{q\pi}{\sqrt{n_0^2 + (n_q + 1)}}, \quad q = 1,2,3, \ldots . \tag{3.2}$$

From here we see the role of q introduced in Eq. (3.1); for fixed values of Θ and n_0, q is indexing the blocks along the main diagonal of the field density matrix as shown in Fig. 2. It is also clear that initial states located in different blocks must evolve to different steady states. Therefore, corresponding to each partition along the diagonal there must be at least one steady-state solution. These steady states of the coherently pumped micromaser, using resonant pumping, were found by Slosser *et al.* [16,17]. They showed that under the trapping-state condition, in the absence of cavity losses, inside each partition (located on the diagonal of the density matrix) the field evolves to pure states, which they called tangent and cotangent states. We note that in this case $\boldsymbol{\beta}$ alone does not uniquely determine the steady state of the micromaser field; different initial conditions lead to different steady states. Therefore, to produce a selected tangent or cotangent state of the field one must carefully prepare an initial state which only extends into the partition where the desired steady state is located. This also means that thermal states cannot be used as initial states in order to generate tangent or cotangent states of the field.

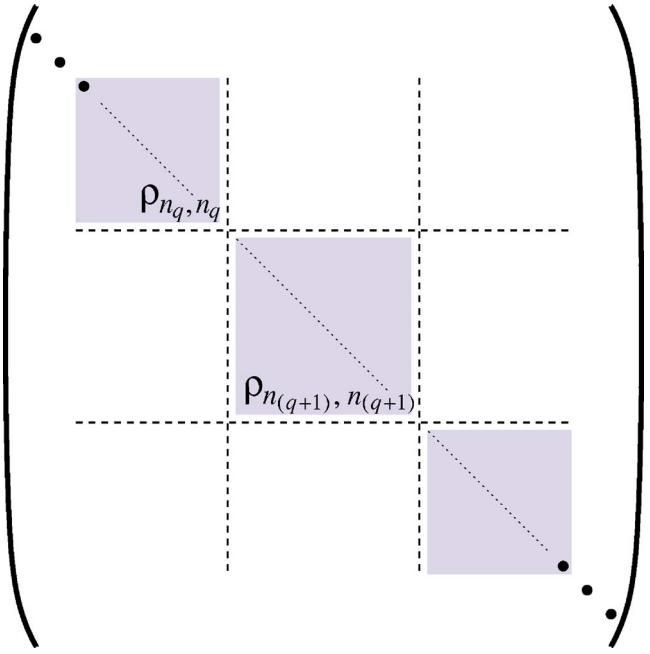

FIG. 2. (Color online) The partitions formed in the field density matrix of a coherently pumped micromaser under trapping-state condition (3.1). Dashed lines indicate the positions where the interaction between neighboring entries is severed. We indicated the upward trapping states located at the lower right corners of the partitions along the main diagonal (noted with the dotted line) of the field density matrix. We also highlighted these partitions along the main diagonal; they in the case of the coherently and resonantly pumped lossless micromaser hold the tangent and cotangent states.

To produce a steady state which is determined uniquely by setting $\boldsymbol{\beta}$ we add the decay process (a thermal reservoir) to the previous system, while we keep the trapping-state condition satisfied. Interaction with the thermal reservoir introduces coupling between the entries of the same diagonal of the field density matrix. In particular, when the thermal reservoir is at zero temperature, the interaction serves as a decay channel to all but the $\rho_{0,0}(\boldsymbol{\beta},t')$ entry of the density matrix. As a consequence all but the entries in the partition that includes the nondecaying vacuum state decay over time. Thus, in the presence of the thermal reservoir, setting $\boldsymbol{\beta}$ unambiguously determines the steady state of the system. Regardless of the initial state of the cavity field, the steady state is always formed in the first partition along the diagonal of the field density matrix. Next, we show how to obtain the analytic solution describing this state of the field. Note that the steady state is not expected to look like a pure tangent or cotangent state seen earlier since the decay process transfers information from the decaying partitions into the nondecaying one. We will discuss the purity of the steady state by showing examples in Sec. IV.

B. Steady-state solution

After understanding the large-scale structure of the field density matrix of the coherently and nonresonantly pumped

lossy micromaser now we present an analytic method which generates the steady-state field density matrix. This analytic method is an extension of the one used in the case of the incoherently pumped micromaser and easily adaptable to supply high-speed numerical algorithms.

In the following we assume that Θ satisfies Eq. (3.2) and that the thermal reservoir, to which the micromaser is coupled, is at zero temperature. Under these conditions, as we discussed earlier, the steady state of the field is localized in the first partition along the diagonal of the density matrix. This partition is bounded by downward trapping state $|0\rangle$ and upward trapping state $|n_q\rangle$. We note that by limiting our investigation to only those interaction phases given by Eq. (3.2), we do not restrict the generality of the discussion. From Eq. (3.2) we see that even in the case when Θ does not satisfy the condition we can still find, by choosing q and n_q appropriately, a Θ_T such that $|\Theta-\Theta_T|<\varepsilon$, which will satisfy Eq. (3.2). This means that we can approximate any steady state of the coherently and nonresonantly pumped lossy micromaser with a state localized in the nondecaying partition of the field density matrix bounded by $\rho_{0,0}$ and ρ_{n_q,n_q}.

To give the steady state we now calculate the $\rho_{k,l}(\boldsymbol{\beta})$ $(k,l=0,1,2,\ldots,n_q)$ entries using the steady-state condition

$$\frac{d\rho_{k,l}(\boldsymbol{\beta},t')}{dt'}=0, \quad k,l=0,1,2,\ldots,n_q. \tag{3.3}$$

To explain how the method works let us assume, for a moment, that we know all $\rho_{k,0}=\rho_{0,k}^{*}$ $(k=0,1,2,\ldots,n_q)$ entries of the field density matrix (the boundary values). If so, by solving simple linear equations $d\rho_{k,0}/dt'=0$ $(k=0,1,2,\ldots,n_q-1)$, one by one starting with $k=0$, we can express the $\rho_{k+1,1}$ $(k=0,1,2,\ldots,n_q-1)$ entries in terms of the boundary values. In addition, we also obtain a condition which must be satisfied by the boundary values from $d\rho_{n_q,0}/dt'=0$; cf. Fig. 3. By repeating the same procedure starting on the main diagonal and moving down along the first column of the field density matrix, we determine the second column of the density matrix (using $d\rho_{k,1}/dt'=0$ we calculate the $\rho_{k+1,2}$ entries for $k=1,2,\ldots,n_q-1$ as functions of the boundary values and obtain an additional condition for the boundary values from $d\rho_{n_q,1}/dt'=0$). After successive repetition of this tedious but simple procedure for the first n_q columns, we determined all entries of the density matrix in terms of the n_q+1 boundary values $\rho_{k,0}$ $(k=0,1,2,\ldots,n_q)$ and obtained n_q conditions $d\rho_{n_q,l}/dt'=0$ $(l=0,1,2,\ldots,n_q-1)$ for the boundary values. The $d\rho_{n_q,n_q}/dt'=0$ equation, which is supposed to deliver the last condition needed to determine the boundary values uniquely, provides no new information because of the structure of Eq. (2.3), since for the diagonal entries,

$$\frac{d\rho_{k,k}(\boldsymbol{\beta},t')}{dt'}=\mathcal{F}_k-\mathcal{F}_{k+1}, \quad k=0,1,2,\ldots,n_q, \tag{3.4}$$

where

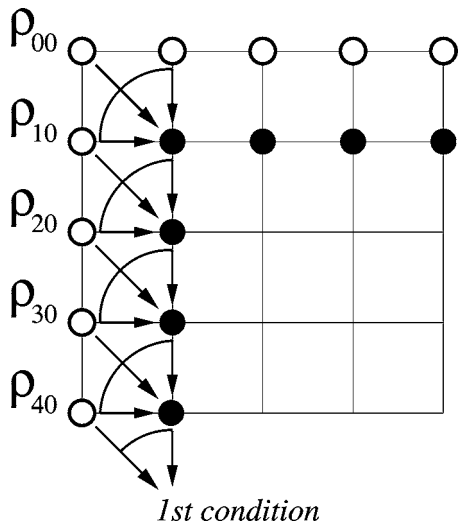

FIG. 3. In the figure ($n_q=4$), we show how to generate each entry in the first column of the field density matrix as a function of the boundary values, represented by the open circles. Starting on the main diagonal and moving down along the zeroth column, after substituting previously generated entries of the field density matrix into the simple linear equation $d\rho_{k,0}/dt'=0$ and solving it for the only unknown $\rho_{k+1,1}$, we determine this as a function of the boundary values. In addition, after substituting the previously determined entries of the field density matrix into $d\rho_{n_q,0}/dt'=0$ we also generate a condition which must be satisfied by the boundary values.

$$\begin{aligned}\mathcal{F}_k=&\left(\frac{N_{ex}}{2}(1+u)S_k^2+\bar{n}_{th}k\right)\rho_{k-1,k-1}(\boldsymbol{\beta},t')\\&+\left(\frac{N_{ex}}{2}\lambda\sqrt{1-u^2}S_kC_k\right)\rho_{k-1,k}(\boldsymbol{\beta},t')\\&+\left(\frac{N_{ex}}{2}\lambda\sqrt{1-u^2}C_k^{*}S_k\right)\rho_{k,k-1}(\boldsymbol{\beta},t')\\&-\left(\frac{N_{ex}}{2}(1-u)S_k^2+(\bar{n}_{th}+1)k\right)\rho_{k,k}(\boldsymbol{\beta},t').\end{aligned} \tag{3.5}$$

Therefore in steady state $\mathcal{F}_k=0$ for $k=1,2,\ldots,n_q$ because $\mathcal{F}_0=0$ which in turn immediately follows from the definition of $\mathcal{F}_k$. Considering that $d\rho_{n_q,n_q}/dt'=\mathcal{F}_{n_q}$ $(\bar{n}_{th}=0)$, it is clear that $d\rho_{n_q,n_q}/dt'=0$ is automatically satisfied and provides no new information. The last equation needed to determine the boundary values uniquely, and thus the whole density matrix, is given by the normalization condition $\Sigma_{k=0}^{n_q}\rho_{k,k}=1$. By solving the n_q+1 conditions we determine all n_q+1 boundary values which, in turn, we use to compute all $\rho_{k,l}(\boldsymbol{\beta})$ entries of the steady-state field density matrix of the coherently pumped micromaser.

The analytic method outlined here is quite straightforward. It involves three steps: First, the generation of each entry of the field density matrix in terms of the boundary values, along with the n_q+1 conditions which must be satisfied by the boundary values; second, solving the n_q+1 conditions to obtain the boundary values; third, substituting the boundary values back to calculate the entries of the steady-state field density matrix. The first and third steps are very

simple; they require only small amount of computational resources even in the case of using symbolic computations. The second step is the computationally most demanding one, but still only requires to solve n_q+1 linear equations to provide each entry of the $(n_q+1)\times(n_q+1)$ field density matrix. (The general method is demonstrated on an example in the Appendix. There, we work out the general analytic solution for the case where the coherently pumped micromaser operates under the trapping-state condition where $n_q=2$.) The simplification is achieved by exploiting the properties of the couplings in the field density matrix and allows us to quickly determine the analytic steady-state field density matrix of the coherently pumped micromaser even for states with $n_q \gg 1$. This method is clearly an extension of the one used in the case of the incoherently pumped micromaser: here we chose all boundary values, not only $\rho_{0,0}$, and generate the conditions to determine them all.

Finally, we point out an important feature of the steady-state solution. Namely, in the case of resonant pumping, when $\omega_{ab}=\nu=\omega_0$, in the steady state all $\rho_{k,l}(\boldsymbol{\beta})$ entries of the field density matrix are real. This can be easily seen, since, in this case, all the linear equations, used to obtain the steady-state values, contain only real coefficients. This feature of the steady state of the field density matrix will have an important implication on the phase of the steady-state field [47].

IV. PHOTON DISTRIBUTION AND THE PURITY OF THE STEADY STATE OF THE COHERENTLY PUMPED MICROMASER

In this section we present some of the results, Figs. 4–11, obtained using the analytic method introduced in Sec. III for investigating the photon distribution of a coherently pumped micromaser under the trapping-state condition where $n_q=28$. Alongside the distributions for the coherently pumped micromaser we also present the results for the incoherently pumped micromaser ($\lambda=0$). To highlight the differences between the two pumping regimes we display the purity of their steady states. The purity of the steady state is characterized by $\mathrm{Tr}[\rho^2]$ and by the normalized entropy

$$S/S_{\max}=\frac{-k_B\mathrm{Tr}[\rho\ln\rho]}{k_B\ln(n_q+1)}, \tag{4.1}$$

where k_B is Boltzmann's constant and $S_{\max}=k_B\ln(n_q+1)$ is the maximum possible entropy of any state in the block to which the steady state is confined. Each result is represented by two graphs. The first, on top, gives the density plot of the micromaser's photon distribution as a function of the atomic inversion u. (In the density plot the black dots indicate the maximum of the photon distribution for given values of u.) The second graph, on the bottom, shows the average photon number ($\langle n\rangle$ in black), the root-mean-square deviation of the photon number (Δn in gray), the normalized entropy ($S/S_{\max}$ in black), and Tr $[\rho^2]$ (in gray) of the steady states. The vertical dashed lines across the graphs indicate the maxima of the root-mean-square deviation, and the solid horizontal gray line denotes the root-mean-square deviation corresponding to the flat distribution. In each graph we have also given all the parameters which were used to generate the results.

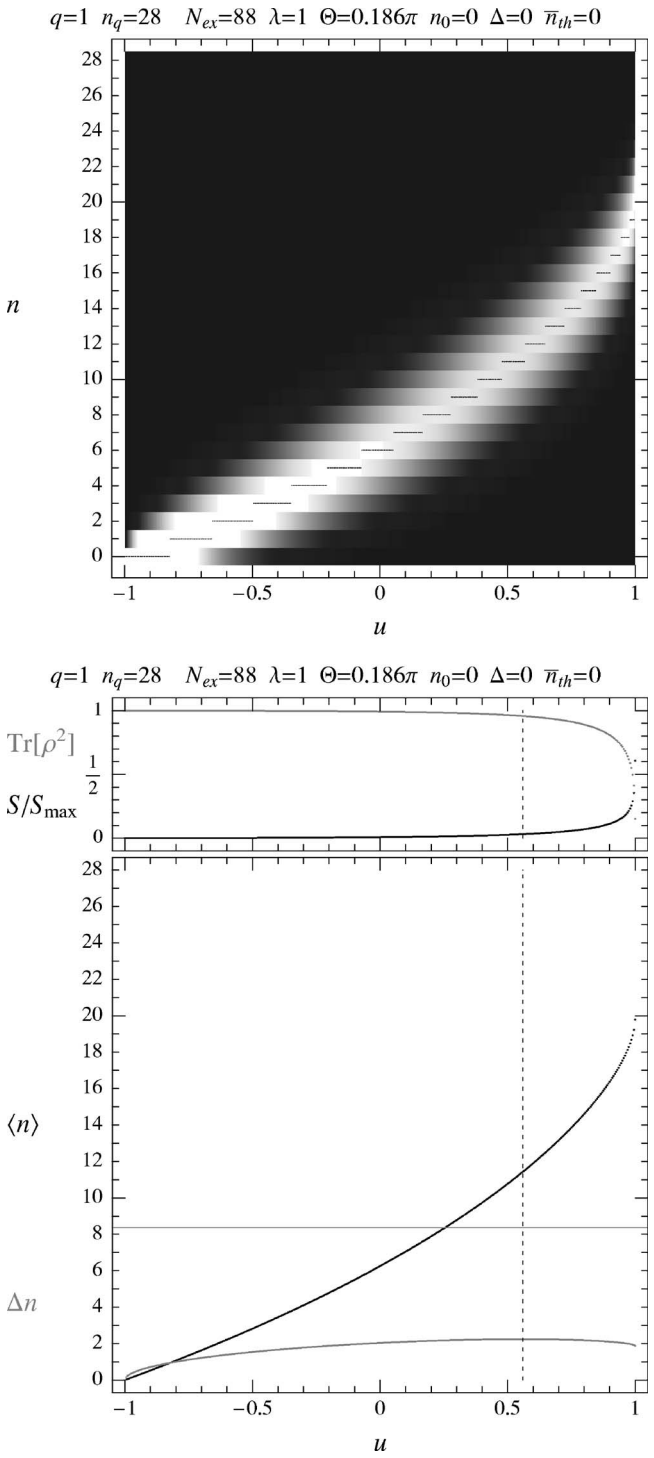

FIG. 4. Results for the coherently pumped micromaser when the interaction phase value Θ is the smallest [$q=1$ in Eq. (3.2)].

In Figs. 4 and 5 we compare the analytic photon statistic of the coherently and incoherently pumped micromaser as a function of the atomic inversion parameter for the smallest possible interaction phase value [$q=1$ in Eq. (3.2)]. In the case of coherent pumping, Fig. 4, we see that the average photon number gradually increases as u increases. From the

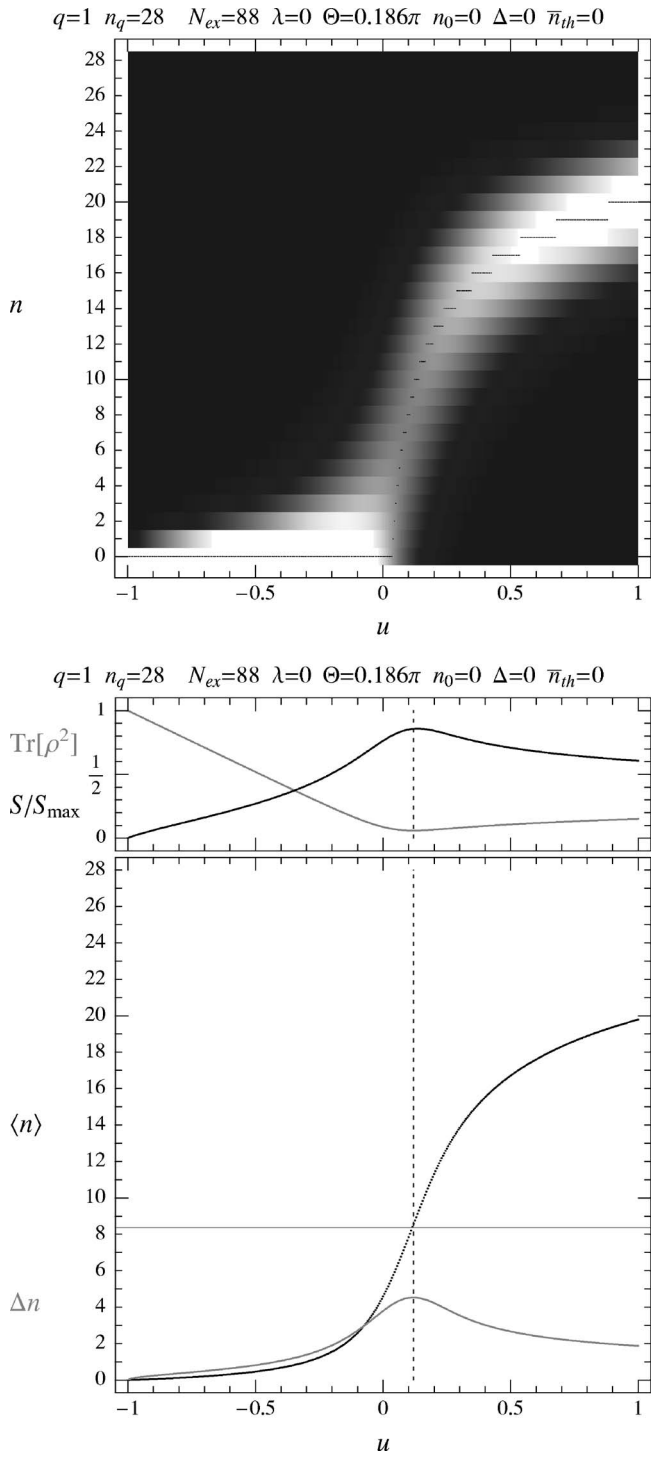

FIG. 5. Results for the incoherently pumped micromaser when the interaction phase value Θ is the smallest [$q=1$ in Eq. (3.2)].

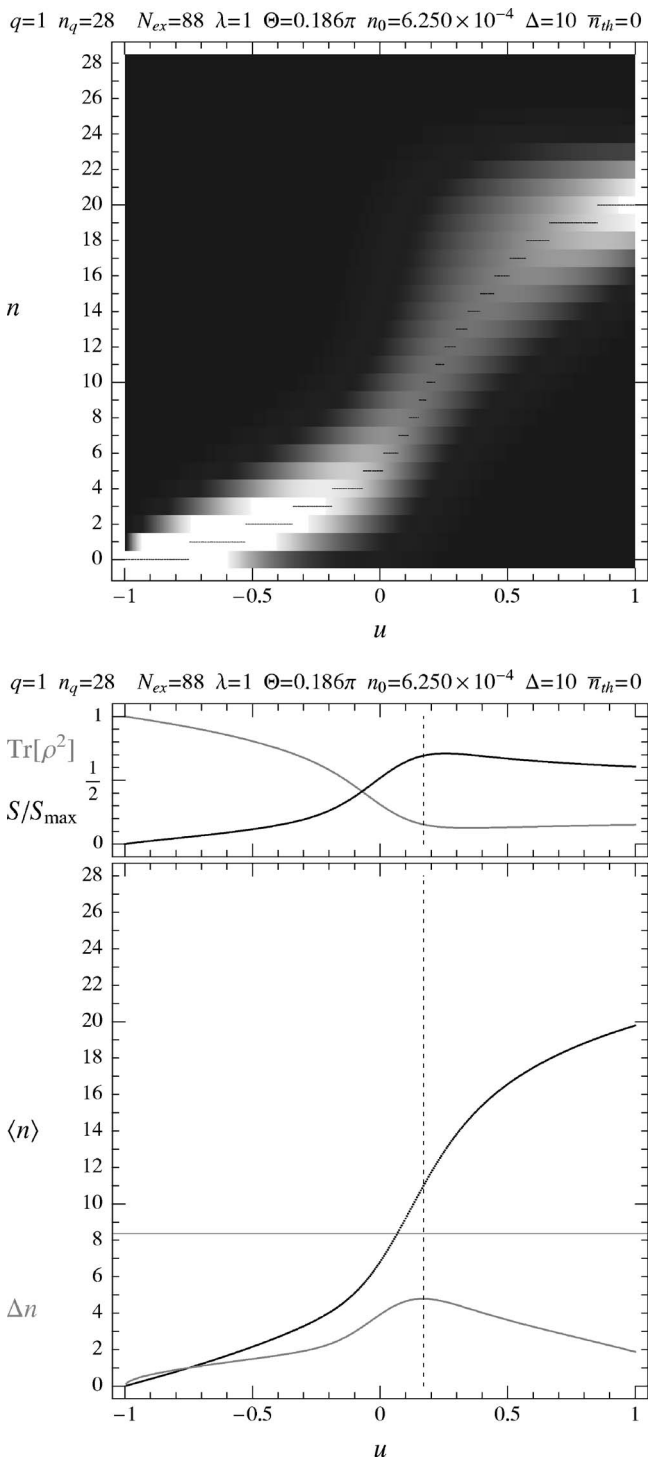

FIG. 6. Results for the nonresonantly and coherently pumped micromaser. We used the same parameters as in Fig. 4 except for the detuning. We assumed that the preparation of the atomic coherence is the most effective and therefore $n_0=(\Gamma/2|g|)\Delta$, with $\Gamma/2|g|=\frac{5}{8}\times 10^{-4}$.

density plot and the root-mean-square deviation of the photon number, which is almost a constant, we conclude that the gradual increase of the average photon number is due to the gradual shift of the field state toward larger photon numbers; no sudden jump occurs. Analyzing the purity of the steady state also reveals that the steady state maintains its high purity for even large values of u; the purity changes only as u approaches 1, where the injected coherence disappears. The incoherently pumped micromaser, Fig. 5, shows a truly different behavior, as u increases the photon number goes through a threshold around $u=0$. From the density plot and the root-mean-square deviation of the photon number we conclude that below the threshold increasing atomic inver-

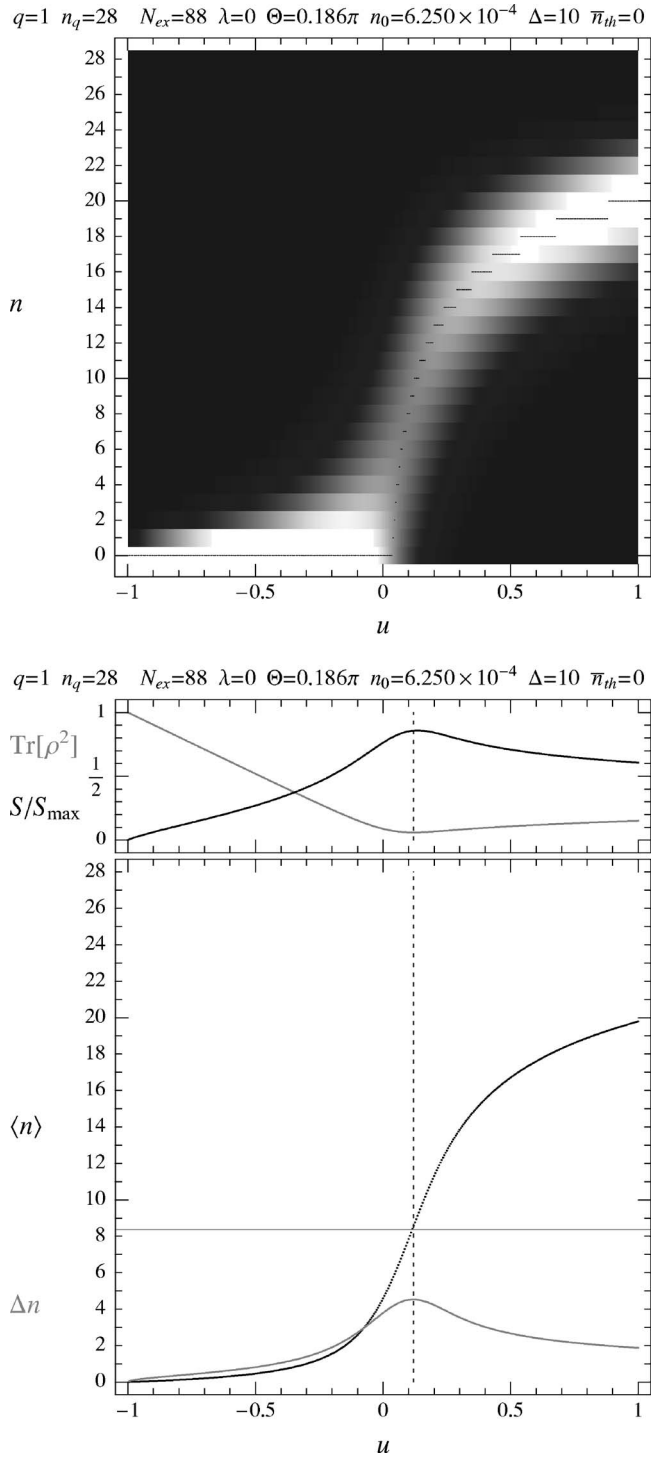

FIG. 7. Results for the nonresonantly and incoherently pumped micromaser. We used the same parameters as in Fig. 4 except for the detuning. We assumed that the preparation of the atomic coherence is the most effective and therefore $n_0=(\Gamma/2|g|)\Delta$, with $\Gamma/2|g|=\frac{5}{8}\times 10^{-4}$.

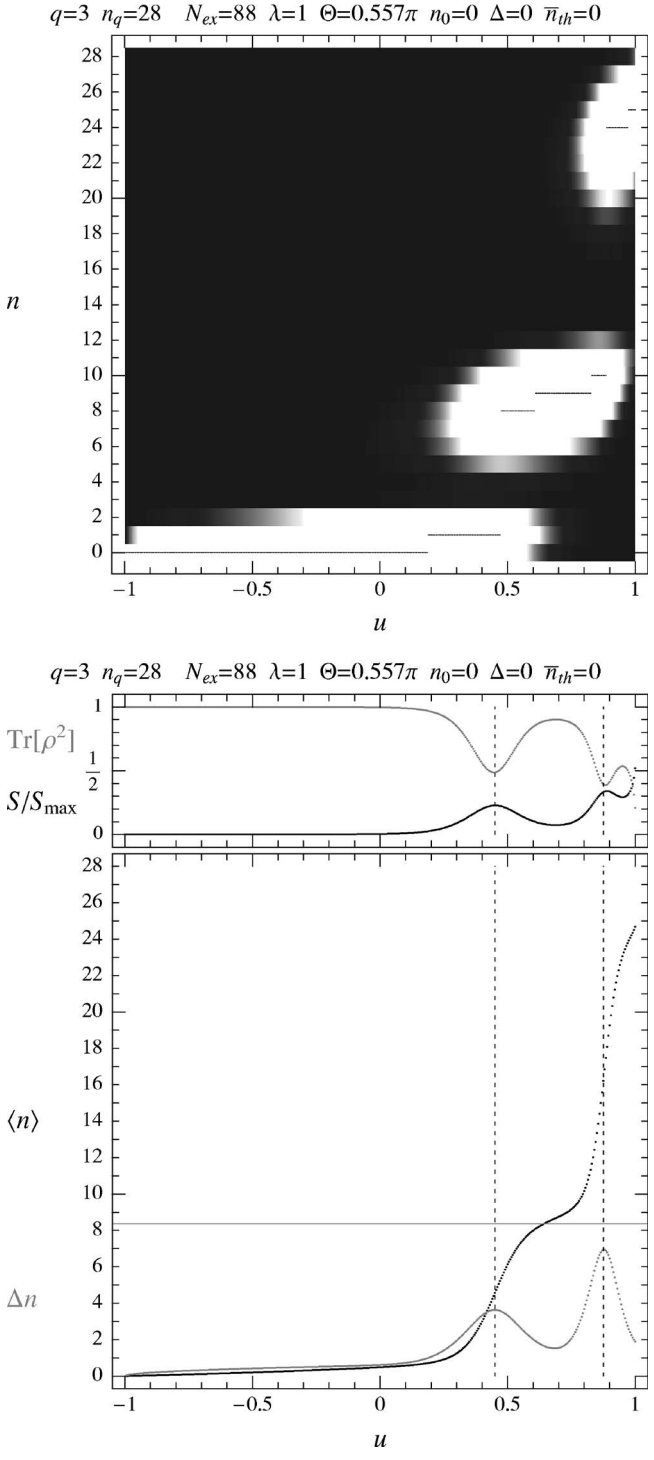

FIG. 8. Results for the coherently pumped micromaser when $q=3$ in Eq. (3.2).

sion does not shift the state of the field toward larger photon numbers, but decreases significantly the purity of the state. Around the threshold a sudden jump in the average photon number occurs which is accompanied by an increase in the root-mean-square deviation of the photon number, indicating a "wide spread" steady state at the threshold, which is also visible on the density plot. Note that the root-mean-square deviation of the photon number and the normalized entropy of the steady state both reach their maxima around the same point near the threshold. Above the threshold, by increasing u, we gradually shift the field state toward larger photon numbers as well as decrease the root-mean-square deviation of the photon number and increase the purity of the steady

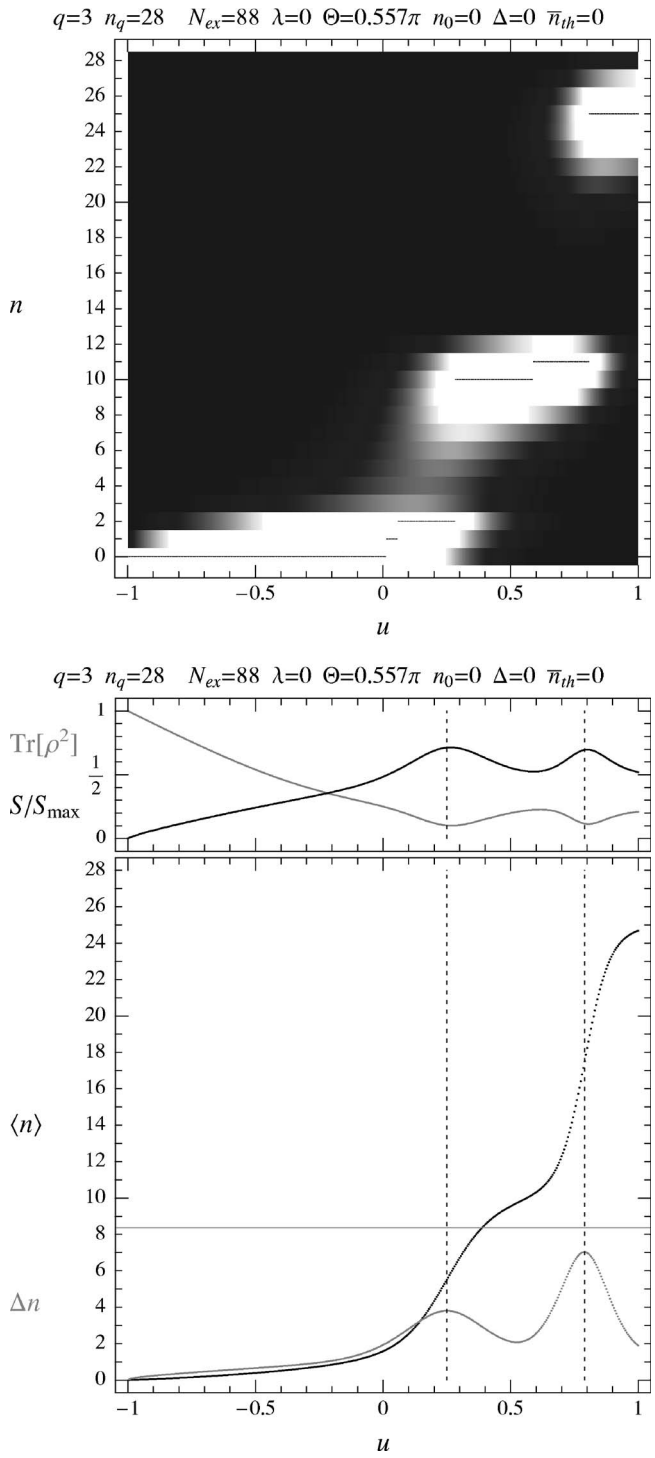

FIG. 9. Results for the incoherently pumped micromaser when $q=3$ in Eq. (3.2).

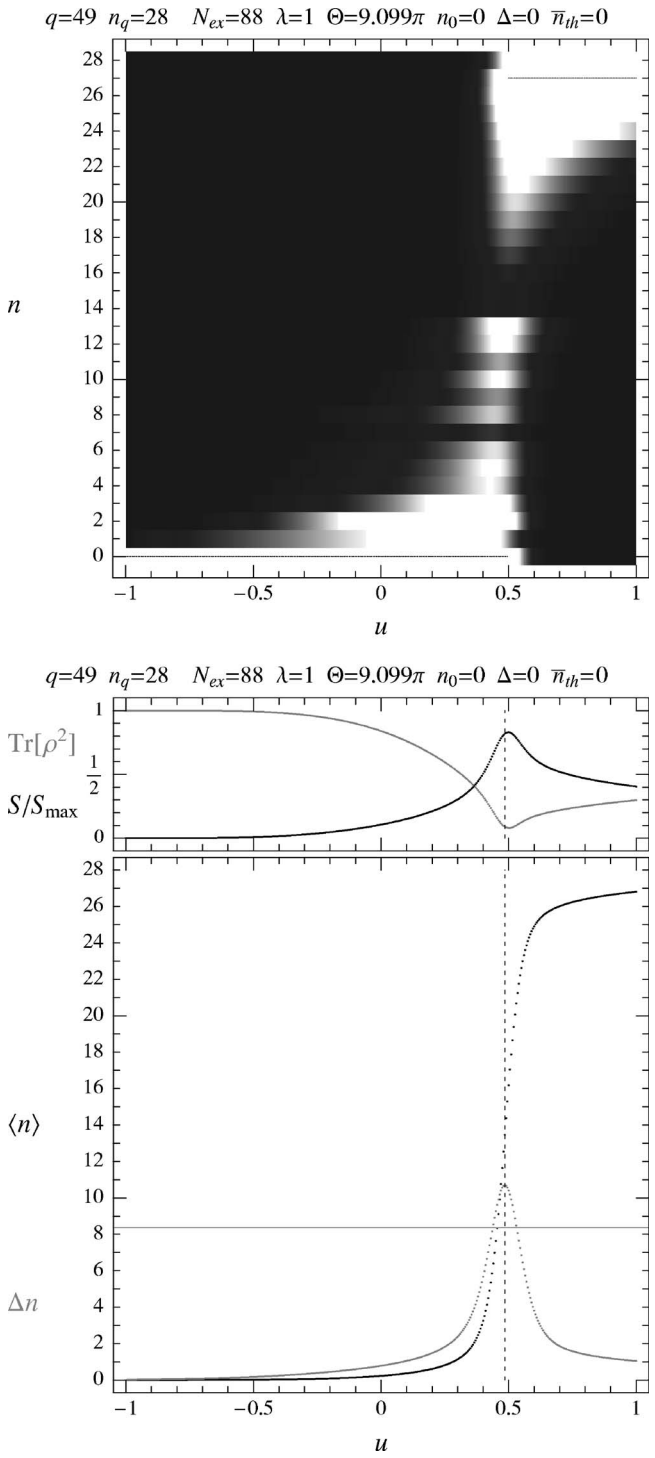

FIG. 10. Results for the coherently pumped micromaser when the interaction phase value Θ is large [$q=49$ in Eq. (3.2)].

state. In conclusion of this example we can say that by injecting coherence we made the pumping more efficient; even in the case of no inversion ($u \leqslant 0$) the field evolved toward a steady state with $\langle n \rangle > 0$. Also the injected coherence helped the system to maintain a high-purity steady state over a wide interval of the atomic inversion parameter.

Next we show how the previous result is affected by detuning. In Figs. 6 and 7 we compare the analytic photon statistic of the nonresonantly and coherently and the nonresonantly and incoherently pumped micromasers. Detuning in the model is controlled by two parameters Δ and n_0. As per our discussion earlier, these are independent parameters. However, the preparation of the atomic coherence is most effective when $n_0=(\Gamma/2|g|)\Delta$, which we assumed here. In Figs. 6 and 7 we show an example where $\Delta=10$; assuming a cavity decay time of 0.2 s translates into a very small (com-

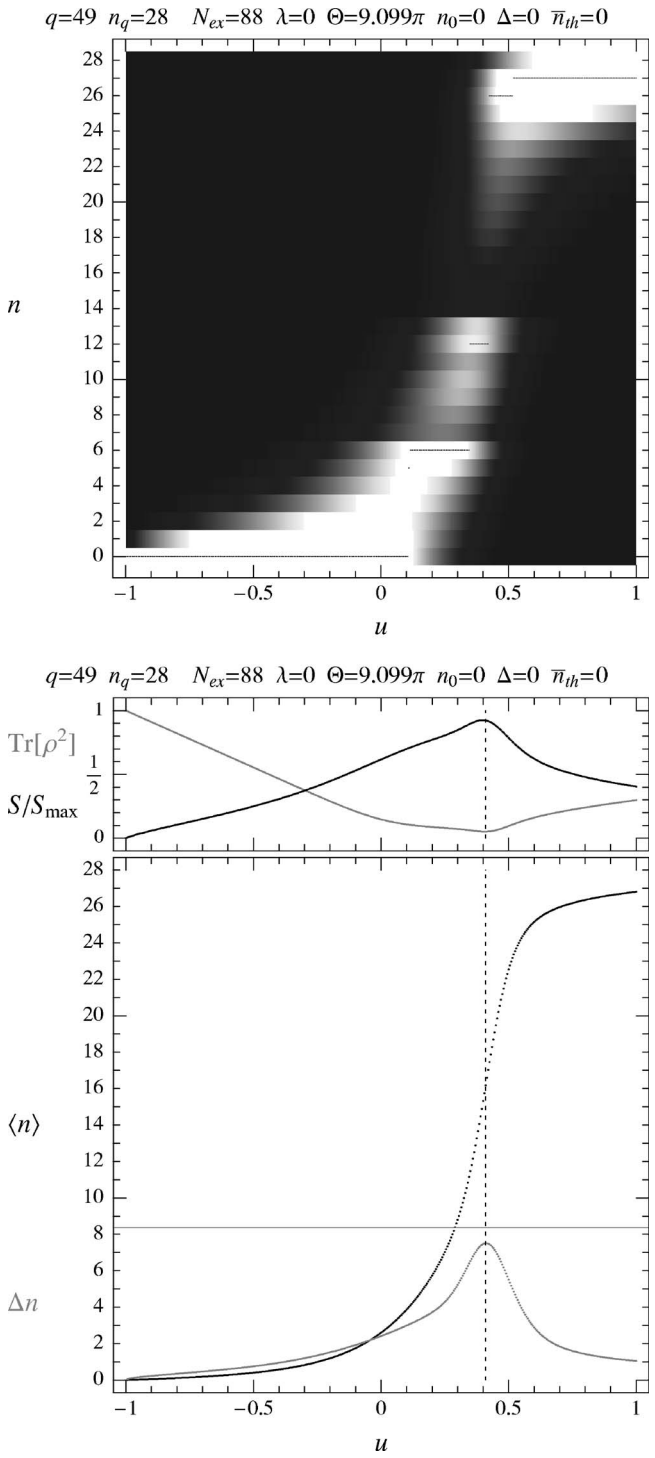

FIG. 11. Results for the incoherently pumped micromaser when the interaction phase value Θ is large [$q=49$ in Eq. (3.2)].

pared to the operational frequency of the micromaser), 50 Hz, difference between the frequency of the empty cavity-field eigenmode and the frequency of the injected signal. The presence of such a small detuning does not noticeably effect the steady state of the incoherently pumped micromaser—this we can see by comparing Figs. 5 and 7—but changes significantly the steady state of the coherently pumped micromaser. Examining Figs. 4 and 6 side by side we conclude that even the presence of a small detuning decreases the effect of the injected coherence significantly; this makes any experimental realizations truly difficult.

Finally, we show what happens to the analytic photon statistic of the coherently and incoherently pumped micromasers as we increase the interaction phase value by increasing q in Eq. (3.2). In Figs. 8 and 9 we show the example where $q=3$. Both in the case of coherent and incoherent pumping as u increases the field goes through $q-1=2$ transitions. Around the transition points in both cases the root-mean-square deviation of the photon number and the normalized entropy of the state increases and between them decreases, indicating where the transitions take place. Even though the basic structures of the transitions look similar, a closer examination of the root-mean-square deviation of the photon number and the normalized entropy of the state reveals that the coherently pumped micromaser "jumps" much quicker between different states (the maxima of the root-mean-square deviation are much narrower) and maintains significantly higher purity between the jumps. Exploiting this feature of the coherently pumped micromaser one can design a "quantum switch:" the u-parameter-induced sudden change between two distinctively different states of the field. In Figs. 10 and 11 we show the photon statistic of a "quantum switch" in the example $q=49$. In this case the field goes through $q-1=48$ transitions as u increases. These transitions in the case of the incoherently pumped micromaser occur over a wide range of u, changing the state of the field gradually. However, as expected, in the case of the coherently pumped micromaser the transitions take place over a much narrower interval of u which makes the field switch suddenly between two distinctively different states. Note that the root-mean-square deviation of the photon number at the transition point increases above the root-mean-square deviation of the flat distribution while the normalized entropy is less than one indicating that the state of the field is composed of number states with high and low photon numbers.

V. SUMMARY

We have presented a comprehensive model of the single-atom micromaser which includes both coherent and incoherent, as well as resonant and off-resonant, pumping. We investigated the large-scale structure of the field density matrix of the coherently pumped micromaser under general conditions; we showed the connections between the trapping states, the tangent and cotangent states, and the steady state of the coherently pumped lossy micromaser formed in the nondecaying partition of the field density matrix. We presented an *analytic* method to obtain the steady state of the micromaser field, which we demonstrated with an example, and presented results provided by the method.

In upcoming articles, we will give a comprehensive *analytic* study of the phase of the micromaser, the semiclassical treatment of the coherently pumped micromaser, and finally the time-dependent *analytic* solution of the master equation (2.3), which we use to generate the spectrum and $g^{(2)}(\tau)$ without applying perturbation theory.

ACKNOWLEDGMENTS

Discussions with B.-G. Englert, Z. Gönye, U. Herzog, M. Hillery, and M. Jakob are gratefully acknowledged. This research was supported by the Office of Naval Research under Grant No. N00014-92-J-1233 and by a grant from PSC-CUNY.

APPENDIX: STEADY STATE UNDER THE TRAPPING-STATE CONDITION WHERE $n_q=2$

This simple, but important example illustrates the method. According to our discussion, we assume that the thermal reservoir to which the micromaser is coupled to is at zero temperature ($\bar{n}_{th}=0$) and that Θ is such that the micromaser operates under the trapping-state condition where $n_q=2$. This means the maximum number of photons the cavity can hold now is 2.

To give the steady-state solution we find all elements of the 3×3 partition of the field density matrix, bounded by $\rho_{0,0}$ and $\rho_{2,2}$, where the steady state is localized. The existing methods call for constructing a complex vector with $(n_q+1)^2=9$ entries from the density matrix and solving the matrix equation obtained from $d\rho/dt'=0$ for the components. This is a brute force method which does not take into account the special coupling of the elements of the field density matrix. Therefore, the method fails to generate an analytic solution even in the case of steady states localized in small nondecaying partitions. Contrary to that, the method proposed in Sec. III exploits the symmetries of the density matrix, reducing the number of equations needed to determine it from $(n_q+1)^2$ to the minimum which is n_q+1. This reduction allows us to find not only the numerical but also the analytic solutions representing the steady states localized even in large nondecaying partitions. (Examples are given in Sec. IV.)

According to the first step described in Sec. III, we generate each entry of the field density matrix in terms of the boundary values and specify the conditions which must be satisfied by the boundary values. Using $\rho_{0,0}/dt'=0$, $\rho_{1,0}/dt'=0$, and $\rho_{1,1}/dt'=0$ we find that

$$\rho_{1,1}=\frac{A^{(2)}_{0,0,0,0}}{A_{0,0,1,1}}\rho_{0,0}+\frac{A_{0,0,1,0}}{A_{0,0,1,1}}\rho_{1,0}+\frac{A_{0,0,0,1}}{A_{0,0,1,1}}\rho_{0,1}$$
$$:=B_{1,1,0,0}\rho_{0,0}+B_{1,1,1,0}\rho_{1,0}+B_{1,1,0,1}\rho_{0,1}, \quad \text{(A1a)}$$

$$\rho_{2,1}=\left(\frac{A_{1,0,0,1}}{A_{1,0,1,1}}B_{1,1,0,0}-\frac{A_{1,0,-1,0}}{A_{1,0,1,1}}\right)\rho_{0,0}+\left(\frac{A_{1,0,0,1}}{A_{1,0,1,1}}B_{1,1,1,0}+\frac{A_{1,0,0,0}}{A_{1,0,1,1}}\right)\rho_{1,0}+\frac{A_{1,0,0,1}}{A_{1,0,1,1}}B_{1,1,0,1}\rho_{0,1}+\frac{A_{1,0,1,0}}{A_{1,0,1,1}}\rho_{2,0}$$
$$:=B_{2,1,0,0}\rho_{0,0}+B_{2,1,1,0}\rho_{1,0}+B_{2,1,0,1}\rho_{0,1}+B_{2,1,2,0}\rho_{2,0}, \quad \text{(A1b)}$$

$$\rho_{2,2}=\left(\frac{A^{(2)}_{1,1,0,0}}{A_{1,1,1,1}}B_{1,1,0,0}+\frac{A_{1,1,0,1}}{A_{1,1,1,1}}B^{*}_{2,1,0,0}+\frac{A_{1,1,1,0}}{A_{1,1,1,1}}B_{2,1,0,0}\right)\rho_{0,0}+\left(\frac{A^{(2)}_{1,1,0,0}}{A_{1,1,1,1}}B_{1,1,1,0}+\frac{A_{1,1,0,1}}{A_{1,1,1,1}}B^{*}_{2,1,0,1}+\frac{A_{1,1,1,0}}{A_{1,1,1,1}}B_{2,1,1,0}\right)\rho_{1,0}$$
$$+\left(\frac{A^{(2)}_{1,1,0,0}}{A_{1,1,1,1}}B_{1,1,0,1}+\frac{A_{1,1,0,1}}{A_{1,1,1,1}}B^{*}_{2,1,1,0}+\frac{A_{1,1,1,0}}{A_{1,1,1,1}}B_{2,1,0,1}\right)\rho_{0,1}+\frac{A_{1,1,1,0}}{A_{1,1,1,1}}B_{2,1,2,0}\rho_{2,0}+\frac{A_{1,1,0,1}}{A_{1,1,1,1}}B^{*}_{2,1,2,0}\rho_{0,2}$$
$$:=B_{2,2,0,0}\rho_{0,0}+B_{2,2,1,0}\rho_{1,0}+B_{2,2,0,1}\rho_{0,1}+B_{2,2,2,0}\rho_{2,0}+B_{2,2,0,2}\rho_{0,2}. \quad \text{(A1c)}$$

Furthermore, using $\rho_{2,0}/dt'=0$ and $\rho_{2,1}/dt'=0$ along with the normalization condition $\rho_{0,0}+\rho_{1,1}+\rho_{2,2}=1$ we find the equations which must be satisfied by the boundary values:

$$0=A_{2,0,0,1}B_{2,1,0,0}\rho_{0,0}+(A_{2,0,0,1}B_{2,1,1,0}-A_{2,0,-1,0})\rho_{1,0}+A_{2,0,0,1}B_{2,1,0,1}\rho_{0,1}+(A_{2,0,0,1}B_{2,1,2,0}+A_{2,0,0,0})\rho_{2,0}$$
$$:=D_{1,0,0}\rho_{0,0}+D_{1,1,0}\rho_{1,0}+D_{1,0,1}\rho_{0,1}+D_{1,2,0}\rho_{2,0}, \quad \text{(A2a)}$$

$$0=(A_{2,1,-1,0}B_{1,1,0,0}-A_{2,1,0,0}B_{2,1,0,0}-A_{2,1,0,1}B_{2,2,0,0})\rho_{0,0}+(A_{2,1,-1,-1}+A_{2,1,-1,0}B_{1,1,1,0}-A_{2,1,0,0}B_{2,1,1,0}-A_{2,1,0,1}B_{2,2,1,0})\rho_{1,0}+(A_{2,1,-1,0}B_{1,1,0,1}-A_{2,1,0,0}B_{2,1,0,1}-A_{2,1,0,1}B_{2,2,0,1})\rho_{0,1}+(A_{2,1,0,-1}-A_{2,1,0,0}B_{2,1,2,0}-A_{2,1,0,1}B_{2,2,2,0})\rho_{2,0}-(A_{2,1,0,1}B_{2,2,0,2})\rho_{0,2}$$
$$:=D_{2,0,0}\rho_{0,0}+D_{2,1,0}\rho_{1,0}+D_{2,0,1}\rho_{0,1}+D_{2,2,0}\rho_{2,0}+D_{2,0,2}\rho_{0,2}, \quad \text{(A2b)}$$

$$1=(1+B_{1,1,0,0}+B_{2,2,0,0})\rho_{0,0}+(B_{1,1,1,0}+B_{2,2,1,0})\rho_{1,0}+(B_{1,1,0,1}+B_{2,2,0,1})\rho_{0,1}+B_{2,2,2,0}\rho_{2,0}+B_{2,2,0,2}\rho_{0,2}$$
$$:=D_{3,0,0}\rho_{0,0}+D_{3,1,0}\rho_{1,0}+D_{3,0,1}\rho_{0,1}+D_{3,2,0}\rho_{2,0}+D_{3,0,2}\rho_{0,2}. \quad \text{(A2c)}$$

Next, we solve the "boundary conditions," Eqs. (A2), for the boundary values and obtain

$$\rho_{0,0}=\frac{\det\begin{pmatrix} D_{1,1,0} & D_{1,0,1} & D_{1,2,0} & 0 \\ D^{*}_{1,0,1} & D^{*}_{1,1,0} & 0 & D^{*}_{1,2,0} \\ D_{2,1,0} & D_{2,0,1} & D_{2,2,0} & D_{2,0,2} \\ D^{*}_{2,0,1} & D^{*}_{2,1,0} & D^{*}_{2,0,2} & D^{*}_{2,2,0} \end{pmatrix}}{D}, \quad \text{(A3)}$$

$$\rho_{1,0} = \frac{-\det\begin{pmatrix} D_{1,0,0} & D_{1,0,1} & D_{1,2,0} & 0 \\ D^*_{1,0,0} & D^*_{1,1,0} & 0 & D^*_{1,2,0} \\ D_{2,0,0} & D_{2,0,1} & D_{2,2,0} & D_{2,0,2} \\ D^*_{2,0,0} & D^*_{2,1,0} & D^*_{2,0,2} & D^*_{2,2,0} \end{pmatrix}}{D}, \quad \text{(A4)}$$

and

$$\rho_{2,0} = \frac{-\det\begin{pmatrix} D_{1,0,0} & D_{1,1,0} & D_{1,0,1} & 0 \\ D^*_{1,0,0} & D^*_{1,0,1} & D^*_{1,1,0} & D^*_{1,2,0} \\ D_{2,0,0} & D_{2,1,0} & D_{2,0,1} & D_{2,0,2} \\ D^*_{2,0,0} & D^*_{2,0,1} & D^*_{2,1,0} & D^*_{2,2,0} \end{pmatrix}}{D}, \quad \text{(A5)}$$

where

$$D = \det\begin{pmatrix} D_{1,0,0} & D_{1,1,0} & D_{1,0,1} & D_{1,2,0} & 0 \\ D^*_{1,0,0} & D^*_{1,0,1} & D^*_{1,1,0} & 0 & D^*_{1,2,0} \\ D_{2,0,0} & D_{2,1,0} & D_{2,0,1} & D_{2,2,0} & D_{2,0,2} \\ D^*_{2,0,0} & D^*_{2,0,1} & D^*_{2,1,0} & D^*_{2,0,2} & D^*_{2,2,0} \\ D_{3,0,0} & D_{3,1,0} & D_{3,0,1} & D_{3,2,0} & D_{3,0,2} \end{pmatrix}. \quad \text{(A6)}$$

Finally, after substituting the proper boundary values, Eqs. (A3)–(A5), into Eq. (A1) we find the analytical solution for the steady state of the coherently and nonresonantly pumped micromaser's field density matrix. Note that this example also demonstrates that the method can be easily transformed into an analytic algorithm, which, together with symbolic computational routines, can be used to find the steady-state solution even if n_q is large.

[1] P. Filipowicz, J. Javanainen, and P. Meystre, J. Opt. Soc. Am. B **3**, 906 (1986).
[2] P. Filipowicz, J. Javanainen, and P. Meystre, Phys. Rev. A **34**, 3077 (1986).
[3] J. A. Bergou, B.-G. Englert, M. Lax, M. O. Scully, H. Walther, and M. S. Zubairy, in *Handbook of Optics*, 2nd ed., edited by M. Bass (McGraw-Hill, New York, 2001), Vol. IV, Chap. 26.
[4] D. Meschede, H. Walther, and G. Muller, Phys. Rev. Lett. **54**, 551 (1985).
[5] M. Brune, J. M. Raimond, P. Goy, L. Davidovich, and S. Haroche, Phys. Rev. Lett. **59**, 1899 (1987).
[6] G. Rempe, H. Walther, and N. Klein, Phys. Rev. Lett. **58**, 353 (1987).
[7] G. Rempe, F. Schmidt-Kaler, and H. Walther, Phys. Rev. Lett. **64**, 2783 (1990).
[8] G. Rempe and H. Walther, Phys. Rev. A **42**, 1650 (1990).
[9] E. T. Jaynes and F. W. Cummings, Proc. IEEE **51**, 89 (1963).
[10] B. W. Shore and P. L. Knight, J. Mod. Opt. **40**, 1195 (1993).
[11] P. Masiak, K. Rzazewski, and L. Roso, Phys. Rev. A **51**, 3267 (1995).
[12] C. Bracher, J. Phys. B **30**, 2717 (1997).
[13] J. A. Bergou and M. Hillery, Phys. Rev. A **55**, 4585 (1997).
[14] P. Meystre, G. Rempe, and H. Walther, Opt. Lett. **13**, 1078 (1988).
[15] M. Weidinger, B. T. H. Varcoe, R. Heerlein, and H. Walther, Phys. Rev. Lett. **82**, 3795 (1999).
[16] J. J. Slosser, P. Meystre, and S. L. Braunstein, Phys. Rev. Lett. **63**, 934 (1989).
[17] J. J. Slosser and P. Meystre, Phys. Rev. A **41**, 3867 (1990).
[18] S. Brattke, B. T. Varcoe, and H. Walther, Opt. Express **8**, 131 (2001).
[19] S. Brattke, B. T. H. Varcoe, and H. Walther, Phys. Rev. Lett. **86**, 3534 (2001).
[20] M. O. Scully, H. Walther, G. S. Agarwal, T. Quang, and W. Schleich, Phys. Rev. A **44**, 5992 (1991).
[21] W. C. Schieve and R. R. McGowan, Phys. Rev. A **48**, 2315 (1993).
[22] T. Quang, G. S. Agarwal, J. Bergou, M. O. Scully, H. Walther, K. Vogel, and W. P. Schleich, Phys. Rev. A **48**, 803 (1993).
[23] N. Lu, Opt. Commun. **103**, 315 (1993).
[24] N. Lu, Phys. Rev. A **47**, 1347 (1993).
[25] K. Vogel, W. P. Schleich, M. O. Scully, and H. Walther, Phys. Rev. A **48**, 813 (1993).
[26] R. R. McGowan and W. C. Schieve, Phys. Rev. A **55**, 3813 (1997).
[27] R. R. McGowan and W. C. Schieve, Phys. Rev. A **59**, 778 (1999).
[28] U. Herzog and J. A. Bergou, Phys. Rev. A **62**, 063814 (2000).
[29] J. Krause, M. O. Scully, and H. Walther, Phys. Rev. A **34**, 2032 (1986).
[30] R. J. Brecha, A. Peters, C. Wagner, and H. Walther, Phys. Rev. A **46**, 567 (1992).
[31] C. Wagner, R. J. Brecha, A. Schenzle, and H. Walther, Phys. Rev. A **46**, R5350 (1992).
[32] C. Wagner, R. J. Brecha, A. Schenzle, and H. Walther, Phys. Rev. A **47**, 5068 (1993).
[33] H.-J. Briegel, B.-G. Englert, N. Sterpi, and H. Walther, Phys. Rev. A **49**, 2962 (1994).
[34] B.-G. Englert, T. Gantsog, A. Schenzle, C. Wagner, and H. Walther, Phys. Rev. A **53**, 4386 (1996).
[35] F. Casagrande, A. Lulli, and V. Santagostino, Phys. Rev. A **65**, 023809 (2002).
[36] F. Casagrande and A. Lulli, J. Opt. B: Quantum Semiclassical Opt. **4**, S260 (2002).
[37] F. Casagrande, A. Ferraro, A. Lulli, R. Bonifacio, E. Solano, and H. Walther, Phys. Rev. Lett. **90**, 183601 (2003).
[38] P. Lougovski, F. Casagrande, A. Lulli, B.-G. Englert, E. Solano, and H. Walther, Phys. Rev. A **69**, 023812 (2004).
[39] N. Lu and J. A. Bergou, Phys. Rev. A **40**, 237 (1989).
[40] J. Bergou, L. Davidovich, M. Orszag, C. Benkert, M. Hillery, and M. O. Scully, Opt. Commun. **72**, 82 (1989).
[41] J. Bergou, L. Davidovich, M. Orszag, C. Benkert, M. Hillery, and M. O. Scully, Phys. Rev. A **40**, 5073 (1989).
[42] J. D. Cresser, Phys. Rev. A **46**, 5913 (1992).
[43] U. Herzog, Phys. Rev. A **52**, 602 (1995).
[44] M. Orszag, *Quantum Optics*, 1st ed. (Springer, Berlin, 2000), Chap. 11.
[45] T. Carty and M. Sargent III, Phys. Rev. A **42**, 1532 (1990).
[46] T. Carty and M. Sargent III, Phys. Rev. A **42**, 1544 (1990).
[47] I. Németh and J. A. Bergou (unpublished).